Distribution Agreement

In presenting this thesis as a partial fulfillment of the requirements for a degree from Emory University, I hereby grant to Emory University and its agents the non-exclusive license to archive, make accessible, and display my thesis in whole or in part in all forms of media, now or hereafter now, including display on the World Wide Web. I understand that I may select some access restrictions as part of the online submission of this thesis. I retain all ownership rights to the copyright of the thesis. I also retain the right to use in future works (such as articles or books) all or part of this thesis.

Hyun Seong Seo April 20, 2020

Fiber Photometry to Assess the Activity Patterns of Supramammillary Nos1 Neurons During Sleep, Wakefulness and Spontaneous Behavior in Mice

by

Hyun Seong Seo

Nigel P. Pedersen MD
Adviser

Biology

Nigel P. Pedersen MD

Adviser

Ken Berglund, PhD

Committee Member

Samuel J. Sober PhD

Committee Member

2020

Fiber Photometry to Assess the Activity Patterns of Supramammillary Nos1 Neurons During Sleep, Wakefulness and Spontaneous Behavior in Mice

By

Hyun Seong Seo

Nigel P. Pedersen MD

Adviser

An abstract of
a thesis submitted to the Faculty of Emory College of Arts and Sciences
of Emory University in partial fulfillment
of the requirements of the degree of
Bachelor of Science with Honors

Biology Program

2020

Abstract

Fiber Photometry to Assess the Activity Patterns of Supramammillary Nos1 Neurons During Sleep, Wakefulness and Spontaneous Behavior in Mice

By Hyun Seong Seo

Recent research from our laboratory has shown that the caudal hypothalamus, specifically the supramammillary nucleus (SuM), is a key and necessary node of the ascending arousal system, and sleep-wake regulatory system. Prior research has shown that there are different cell types in the SuM; glutamate-releasing neurons in the SuM can drive wakefulness, while neuronal cells containing nitric oxide synthase (NOS) appear to be important for rapid eye movement (REM)-related cortical activity, and the GABA/glutamate-containing population targets the hippocampus, densely innervating the dentate gyrus and CA2. Thus, the SuM has at least three populations of apparently functionally distinct neurons. While our prior work has been based on manipulations of these cellular groups, we have not examined the spontaneous activity of these neuronal groups during various states of arousal. To achieve this, we use the technique known as fiber photometry, permitting the real-time assay of calcium fluxes, as a proxy for neural activity, in genetically-targeted SuM neuronal groups. We will then correlate this activity with different behaviors and sleep-wake state changes in order to understand sleep-wake related activity in the different cellular populations within the SuM.

Fiber Photometry to Assess the Activity Patterns of Supramammillary Nos1 Neurons During Sleep, Wakefulness and Spontaneous Behavior in Mice

By

Hyun Seong Seo

Nigel P. Pedersen MD

Adviser

A thesis submitted to the Faculty of Emory College of Arts and Sciences
of Emory University in partial fulfillment
of the requirements of the degree of
Bachelor of Science with Honors

Biology Program

2020

Acknowledgements

I would like to personally thank our lab members Lauren Aiani, Katherine Zhu, and Dr. Adam Dickey for their assistance for this study. Lauren performed the surgical procedures, trained me on the different procedures from sleep scoring to histological processing. Furthermore, she also oversaw animal care and breeding of the Nos1 – Cre animals used in this project. Katherine printed and processed the headplates required for the recordings of EEG/EMG. Dr. Adam Dickey wrote and helped troubleshoot the code required for the analysis required for the data. I would also lastly like to thank my advisor, Dr. Nigel Pedersen for his great support and guidance during my time in the lab and as an honor student.

Table of Contents

Introduction

Background of Sleep

Sleep is a defining characteristic of mammals and various invertebrates. Humans typically spend 7 – 8 hours on average asleep per day, meaning a third of their lives are spent in this state (Carskadon et al., 2005). There generally accepted to be three states of sleep-wake in rodents: wakefulness, non–REM (non rapid eye movement) sleep, and rapid-eye movement (REM) sleep. While non–REM sleep (or sometimes referred to as slow wave sleep in rodents) is separated further into 3-4 stages in humans, depending on scoring criteria, it is overall characterized in humans and rodents as a state with period of reduced activity and mentation with higher amplitude lower frequency waves in an electroencephalogram (EEG) (Purves, 2001). On the other hand, REM or paradoxical sleep is characterized in both humans and rodents by periodic intervals of rapid eye movements with wake-like cortical activity (low voltage and high frequency waves) and muscle atonia, or loss of tone in non-respiratory muscles (Siegal, 2005). Sleep occurs in a cycle transitioning from each state throughout the night (Weitzman, 1972). In humans, a typical 8 hours of sleep for a night would on average lead to five 90-minute sleep cycles, each ending with a period of REM sleep, with time spent in REM progressively increasing throughout the night (Purves, 2001). In rodents, sleep cycles of a specific duration are not evident, but periods of non-REM tend to transition to REM before arousal. The overall purpose of sleep is subject to debate, but it is clearly an essential restorative process for both physical and emotional health, molecular synthesis and tissue-level repair; sleep deprivation, conversely, in animal models have led to multi-organ damage and impaired cognition, attention and memory consolidation (Periasmy et al., 2015). Furthermore, the purpose of REM sleep and dreaming maintains an open question and is not fully understood. REM sleep is known for its

importance in brain development in young mammals and its significance in memory consolidation as behavioral testing of inhibiting REM sleep has led to memory deficits (Blumberg, 2010; Diekelmann, 2010). Furthermore, the prevalence of muscle twitches in REM sleep has been linked to development of sensory motor system (Blumberg et al., 2013). Another hypothesis claims that REM sleep is a method for the brain to wake up from prolonged periods of unconsciousness as wake and REM sleep share similar brain activity and likely originate from a similar brainstem arousal pathway (Klemm, 2011). In the process of further understanding this question, research into the mechanisms and neuronal circuitry that allow for the transition between sleep and wake states are being investigated, including in the present studies.

Background of the Ascending Arousal System

Transitions from sleep to wake correlate with the appearance of lower-amplitude high-frequency EEG activity from the slow background activity of sleep (Moruzzi and Magoun, 1949). These physiological changes found during arousal situations were mimicked in experiments with anesthetized animals where the direct stimulation of a specific region in the brain stem could replicate EEG waves found in arousal reactions (Moruzzi and Magoun, 1949; French and Magoun, 1952). Furthermore, experiments of lesions and transections in the brainstem led to comas in cats, further reinforcing its role in arousal (Lindsey et al., 1950). This region of the brain stem was named the reticular formation due its nerve fibers surrounding the neurons, forming a web-like appearance histologically (Parvizi and Damasio, 2001). Because of the early physiological experiments with subcortical stimulation (Moruzzi and Magoun, 1949) and reticular inputs into the forebrain (Parvizi and Damsio, 2001; Morison and Dempsey, 1942), the reticular formation was considered the anatomical substrate of what was termed the “ascending

reticular activating system" (ARAS, Moruzzi and Magoun, 1949). Since the 1950s the term reticular formation has been largely rejected given parcellation of these regions into discrete nuclei (see for example Olzewski and Baxter, 1954), so more recent work typically refers to the ascending arousal system (AAS). The AAS is considered a collection of nuclei that are anatomically and physiologically unique and function through activating neurons in the various nuclei of the formation. However, through later studies, the rostral pons was found to be the origin of the ascending arousal system, as lesions at this level would cause coma in animals (Batini et al., 1959, Parvizi and Damasio, 2001, Fischer et al., 2016).

The pathways of the ascending arousal system were initially found through the tracing experiments of degenerating neurons from the lesions of the reticular formation (Nauta and Kuypers, 1958, Fuller et al., 2011). Overall, there are two main pathways for the ascending arousal system (dorsal arousal network); one innervates the thalamus and the other projects to the lateral hypothalamus and the basal forebrain (ventral arousal network). The main area of innervation to the thalamus are the pedunculopontine and laterodorsal tegmental nuclei (PPT – LDT) (Hallanger and Wainer, 1988), which incorporate cholinergic neurons to project into the different regions of the thalamus, including the intralaminar nuclei of the thalamus which has diverse projections to the different regions of the cerebral cortex, the thalamic relay nuclei, and the reticular nucleus of the thalamus (Groenewegen and Berendse, 1994; Steriade et al., 1993). The neurons in the PPT – LDT have shown to vary in activity based on the different states of sleep and wake. During wakefulness, the neurons are shown to fire at a higher rate and as the individual transitions to sleep, neurons seem to be inhibited and only a few are active (Saper et al., 2001). However, when REM sleep occurs, these neurons once again activate and fire rapidly (Mansari et al., 1989). Despite this, large and even total lesions of the thalamus have been shown

to have minimal effect on the amount of non-REM/REM sleep and EEG/EMG (Electromyogram) patterns (Fuller et al., 2011), but higher frequency cortical activity consistent with cognition is markedly reduced (e.g. Anaclet et al., 2015).

The second route of the ascending arousal system bypasses the thalamus to modulate the activity of the cortex through projections from the basal forebrain and lateral hypothalamus (Saper, 1985; Saper et al., 2001). This particular pathway stems from the upper brainstem and includes the pontine tegmentum, locus coeruleus (LC) containing norepinephrine, dorsal (DR) and median raphe nuclei containing serotonin, tuberomammillary nucleus (TMN) containing histamine, the ventral periaqueductal grey matter containing dopamine, as well as in the hypothalamus, particularly the caudal (as above) and lateral regions (including orexin neurons), as well the basal forebrain containing acetylcholine, GABA and glutamate neurons (Saper, 1985, 1987; Saper et al., 2005; Pedersen et al., 2017; Saper et al., 2009; Anaclet et al., 2015). These nuclei all contribute to the diffuse projections to the cerebral cortex and have different activity patterns depending on the sleep -- wake state (Aston – Jones et al., 1991, McGinty and Harper 1976, Vanni-Mercier et al. 1984). The basal forebrain's neuronal activity has been shown to be maximal during wake and paradoxical sleep and experiments with chemogenetic manipulation have shown that activation sustains wakefulness and inhibition increases sleep (Lee et al., 2005; Anaclet et al., 2015). Furthermore, lesions in the lateral and caudal hypothalamus result in somnolence, but not coma (Nauta, 1946).

The Hypothalamus in the Ascending Arousal System

The role for the hypothalamus in the control of wakefulness has been appreciated for almost a century. In 1917, the Spanish influenza pandemic, passing through much of the world,

was associated with epidemic *encephalitis lethargica*, with patients experiencing a number of syndrome including severe states of sleepiness (Vilensky 2011). This particular disease would cause some patients to sleep for more than 20 hours, only awakening for daily necessities such as food or water (Saper et al., 2005). This particular disease was associated with lesions at the junction between the midbrain and the diencephalon in patients with hypersomnolenia or somnolence (Von Economo, 1917). This was further replicated in monkeys where hypothalamic lesions would induce somnolence (Ranson, 1939). On the other hand, in a small minority of patients afflicted with this disease had the opposite effect and were insomniac, unable to fall asleep even though they were tired. These patients instead had lesions in the basal ganglia and the anterior aspect of the hypothalamus. This state of insomnia was later replicated in subsequent studies where the pre-optic area of the hypothalamus was lesioned (Nauta et al., 1946). Thus, this brought the reasoning that the hypothalamus included both sleep-promoting and wake-promoting neurons in the anterior and posterior hypothalamus, respectively. Recent studies have identified a caudal hypothalamic nucleus, the supramammillary nucleus (SuM), as the long-sought node of the arousal system, as well as the preoptic hypothalamus as promoting sleep (Sherrin et al., 1996).

The supramamillary nucleus has been known for its projections to the cerebral cortex (Saper, 1985), the basal forebrain and the hippocampus (Amaral and Cowan, 1980). The SuM has been shown to control the plasticity and theta activity for the hippocampus (Pan and McNaughton, 2004). Prior research has indicated that there are several distinct cell populations in the SuM which have different roles in modulating vigilance states. Glutamate-releasing neurons of the SuM are shown to promote continual wakefulness when chemogenetically activated and cause somnolence when inactivated (Pedersen et al., 2017). Lesions of the SuM also affect REM-related theta activity in the EEG (Renouard et al., 2015), subsequently

attributed to a subpopulation of nitric oxide synthase and glutamate expressing neurons that can promote wake and are necessary for normal amounts of theta activity in REM sleep (Pedersen et al., 2017). More interestingly, a group of GABA/glutamate neurons which have minimal effect on sleep and wake, are a major source of afferent inputs into the hippocampus of rats and monkeys, especially the dentate gyrus (DG) which has been theorized to act as a "gate" of filtering out excitatory signals, which is injured or dysfunctional in temporal lobe epilepsy, and when activated can lead to the onset of seizures (Krook-Magnuson et al., 2015). This afferent input from the SuM has also been implicated in spatial learning and memory. Recent research has shown that both the SuM and DG neurons have been shown to have higher neuronal activity during spatial memory retrieval tasks as observed through fiber photometry (Li et al., 2020). However, the SuM, and particularly the subpopulation of Nos-containing neurons, has a more defined role in a particular sleep state: rapid eye movement sleep. While these neurons have less significant impact on the overall sleep and wake due to accounting for only around 20% of the SuM Vglut2 neuronal population, their chemogenetic inactivation has a suppressive effect on the theta rhythm that is prevalent in REM sleep. Thus, to further understand the role of Nos1 neurons in the SuM in the different states of sleep and wake, as well as to better understand the neural circuits underlying the REM state and EEG changes, we sought to observe the spontaneous activity of this specific neuronal population without manipulations and in a more naturalistic setting. While this information will be critical for better characterizing REM brain circuits, it pertains to epilepsy given that REM is a state in which temporal lobe seizure are very rare and few or no epileptiform discharges occur (Shouse et al., 2000).

Fiber photometry

Fiber Photometry is a recently created optical technique that incorporates genetically encoded calcium indicators to track changes in intracellular calcium concentrations allowing for the ability to connect neuronal activity to specific behaviors/states of animals (Gunaydin et al., 2014; Calipari et al., 2016). Calcium is a second messenger and has an essential role in propagating action potentials due to calcium influx, with rising somatic concentration during neural activity, as well as triggering the release of neurotransmitters at the axon terminal (Sabatini et al., 2002). Thus, for this technique, calcium activity is taken as a proxy for neural activity allowing for the deeper understanding of the neural dynamics of a certain cell population. This technique is relatively minimally invasive as a single optical fiber is placed in brain structures of interest and is able to both deliver an excitation light and collect light emitted from the fluorophore sensor, GCaMP (Akerboom et al., 2012). Using this technique, one could, for example, target the SuM and observe real time neural activity of Nos1/Vglut2 neurons through the use of a Cre-conditional GCaMP (Dana et al., 2019) in Nos1-Cre mice. This technique allows for the mouse to move freely and be recorded for 24 hours or more and, unlike field potential recording, will give a read out of the activity of a genetically-identified population of neurons. This allows for us to understand the activity of a selected set of previously described neuronal subpopulations during distinct stages of sleep and wake. Furthermore, with the addition of video, EEG, hippocampal field potential and EMG (electromyogram) recordings, it would be possible to validate whether an animal is asleep or awake during the recording interval, as well as correlations with changes in behavior and hippocampal rhythms. Thus, one might obtain an understanding the activity dynamics of the Nos1/Vglut2 cell population and how varying activity can indicate a certain sleep stage or wakefulness.

Rationale and Hypothesis

Through chemogenetic techniques, the activations of certain neuronal cell types in the SuM have been shown to have a role in arousal. However, these have only been manipulations that have been performed on the SuM and neural activity has only been recorded electrophysiologically in anesthetized rodents, thus not revealing the activity of known cell types and not permitting the study of sleep-wake changes in freely behaving activity. Therefore, by using fiber photometry, we can obtain real time recordings of sleep–wake changes and analyze the activity of this specific neuronal cell type. Based principally on lesion and chemogenetic studies described above, we hypothesize that NOS1 neurons will be active during wake but show the highest level of activity during REM sleep.

Materials and Methods

Animals

Both male and female Nos1–Cre animals (20 – 40g, n = 7, 12 – 52 weeks) obtained from the Jackson Laboratories (give catalog number) (and presently available in the Pedersen lab) housed in 12-hour light/dark cycles with ad libitum access to food and water. These animals were single housed following fiber optic and headset placement (Zhu et al., 2020). The experimental protocols were approved by the Emory University IACUC which followed guidelines for the Care and Use of Laboratory Animals from the National Institutes of Health.

Viral Constructs

To achieve cell specific GCaMP expression from Cre transgenic lines, AAV9-Syn-Flex-jGCaMP7s-WPRE (Addgene) was used for this experimental study. This is an adeno-associated, viral vector serotype 9 (AAV9) that is under the control of a neuronally-expressed human synapsin

I promoter (Syn) and flip excision (FLEX) switch (Schnutgen et al., 2003) that allows for genetic Cre-recombinase to allow for the correct orientation to appear and transcription to occur. GCaMP7s is a construct that has a circularly permutated green fluorescence protein and calmodulin, a calcium binding protein (Dana et al., 2019).

Stereotaxic Surgery: Headset Placement and Fiber Placement

Mice were anesthetized with ketamine (100mg/kg) and xylazine (10 mg/kg) diluted in saline through intraperitoneal injection (0.1 mL per 10 grams). Furthermore, they were also given Meloxicam (5mg/kg) in saline up to 1 mL, administered through intrascapular subcutaneous injection. After the mouse is fully anesthetized, depilatory cream was added to efficiently remove fur from the surgical field. Then, Lidocaine (2% in saline) was subcutaneously delivered using a 0.5 ml syringe at the area of incision. The skin was sterilized with three rounds of 70% isopropanol wipe and an iodine wipe. Three incisions were made and excess skin was removed by lateral surgical scissors. The mouse is placed on a Cartesian stereotaxic frame (Cartesian Instruments now Model 1900, Kopf, Tujunga, CA) and holes are drilled for the placement of the screw electrodes for the headset (Frontal: ML: -1.30, AP: 1.00, Ground: ML: 1.30, AP: 1.00, Reference: ML: 0.00, AP: -6.00, Parietal: ML: 2.80, AP: -1.50). Then, the animal is moved to the Neurostar Robot Stereotaxic frame which is computer controlled and atlas integrated to allow for high accuracy stereotaxic injections. A glass capillary pulled to ~30 µm outer diameter was used for the injection of 250 nL of the vector into the medial SuM (ML: 0.05, AP: -2.40 DV: -4.74). Following the microinjection, the headplate described in a recent paper and modified with a cut-away for fiber placement (Zhu et al., 2020) was implanted along with a fiber optic cannulae threaded through a metal ferrule (400 µm core, 0.48 NA). To avoid contact with the headset, the optical fiber and

ferule is placed at a 30 degree angle. Mice were placed into individual recording barrels for 2 weeks after surgery, permitting sufficient GCaMP expression, before they were connected to a preamplifier and commutator (see below) for habituation of 24 hours prior to 24 of recording of video, EEG, hippocampal field potential, EMG and fiber photometry signals.

Headset Recordings

The headset was designed using OpenSCAD software and 3D printed through a resin printer through the Pedersen lab. The headset was assembled to allow for the recording of EEG through frontal-parietal cortical electrodes, and hippocampal microwire electrodes, and EMG through pads which were inserted into the neck muscles. Modified from the standard headset, the version used in these studies had no right hippocampal microwire depth as a cut-away was created to allow for the placement of the fiber optic cannulae (Zhu et al., 2020). For recording, a pinnacle preamplifier (8406-SE31M, 100x gain) and an assisted electric rotary joint (Doric Lenses) that transmits signals for 12 channels were used to record synchronized video and EEG/EMG signals through a Cambridge Electronic Design Power 1401 A-D converter. These signals were saved through Spike2 (Version 9.04b, Cambridge Electronic Design, Cambridge, UK). Data was sampled at 2 kHz and recordings were automatically saved into 6 files with 4 hour blocks (total 24 hour recording).

Fiber Photometry

Prior to each recording, the 400 μm 0.48 N.A. optical fiber (Doric Lenses) was bleached from 8 – 12 hours to prevent autofluorescence from being recorded by the photodetector. The fiber photometry system used was the Doric Fiber photometry system which uses a 465 nm and 405 nm LED lasers sinusoidally modulated at 208.616 Hz and 572.205 Hz respectively. This is

coupled with a 400 μm 0.48 N.A. optical fiber connected, through a fiber optic swivel joint, to the 400 μm 0.48 N.A. fiber cannulae implanted into the brain. The emission was collected through the same optical fiber and passed through a 4 port fluorescence mini-cube (FMC4, Doric Lenses) which allows for locked in detection of the isosbestic and functional excitation; then detected onto a photodetector (Newport Visible Femtowatt Photoreceiver Module). Both the raw data and the demodulated data was recorded in real-time through the Doric Neuroscience studio program, in parallel to combined recording of this data with video and other physiological data with Spike2, as above. This raw data was recorded with Spike2 to allow for precise synchronization and validation of the demodulation of Doric Neuroscience Studio. Fiber photometry signals were collected at a sampling frequency of 10 kHz on both the Doric and CED based systems.

Processing and Immunohistochemistry

At the end of the recordings, these mice were anesthetized with pentobarbital (150 mg/kg) through an intraperitoneal injection. Then, the mouse was then perfused with saline and 10% formalin diluted with PBS (Phosphate Buffered Saline). The headsets were removed before the brains were extracted and placed into 10% formalin for 6 – 8 hours for the post-fixing process. Then, the extracted brain is placed into a 30% sucrose solution for at least 48 hours before sectioning. The brains were blocked and sectioned at 50 μm. These sections were then mounted and coverslipped with Fluromount – G. These slides were observed under a fluorescence microscope for anatomical validation of injection site and fiber optic placement.

Data/Statistical Analysis

The raw data from fiber photometry recorded through Spike2 (Cambridge Electronic Design) was exported to Matlab R2020a (The Mathworks) where the data was low pass filtered with a 6^{th} order butterworth smoothed through a custom made script (Code in appendix of thesis). Then, this processed data was compared for accuracy to the demodulation done by Doric Neuroscience studio. To accommodate for photobleaching, a second degree polynomial was used as a baseline. After processing of each channel, the Sleep-wake scoring based on synchronized video and EEG/EMG recordings done through Spike2 were used to correlate the calcium signals with wakefulness/non-REM/REM states (Kadam et al., 2017, Gao et al., 2016, Costa-Miserachs et al., 2003). Each state of consciousness/unconsciousness was given a number: 1 for Wake, 2 for NREM, and 3 for REM. One number was assigned to each epoch which was 20 seconds long. Then, the average mean of the waveform were calculated for each state of consciousness and normalized based on the range of the signal amplitude. These means were used to run a 1-way ANOVA to observe if there was statistical significant difference among the three groups and a post hoc Tukey-Kramer test was run to compare the individual sleep states.

Results:

Demodulated data and raw data are highly correlated

First, we examined the raw trace and demodulated fiber photometry signal. Manually demodulated raw signal (the smoothed (τ = 1 s) root mean square power in a narrow band centered on 208.616 Hz, for 405 nm laser, and 572.205 Hz, for 465 nm laser, by respective corresponding channel) was examined next to the smoothed (τ = 1 s) or 6^{th} order Butterworth

filtered (5 hz) raw signal and Doric photometry console demodulated signal and found to be highly similar (Pearson R = 0.99). This indicated that our signal has a very high signal to noise ratio, likely due to the complete exclusion of incident light and effective wavelength filters in our set-up, further reinforcing the correlation of neuronal activity to behavioral changes. Thus, with filtering alone and without any further analytical steps, we were able to physically observe the relationships between the calcium indicator, and inferred activity of the neuronal region being recorded, and sleep-wake state.

Stable photometry and EEG/EMG signals were obtained in freely moving mice.

In this study, we were able to successfully utilize fiber photometry to obtain biological signals in freely behaving mice and correlate this activity with behavioral states. We have found that the different states of sleep and wake affect the calcium indicator fluorescence, a proxy of neuronal activity, in the experimental mice. While we have not been able to validate fiber placement and injection sites due to the COVID-related suspension of laboratory activity, we found that in all mice, there were state-related changes in photometry signal that correlated with traditionally scored sleep-wake using EEG/EMG and video. We found that during REM sleep, these mice had higher levels of fluorescence or activity compared to the two other states of consciousness. This was validated by calculating a normalized mean of the wave form during intervals of REM sleep. All experimental animals had noticeably higher normalized mean values for REM compared to the two other tests. Wake, which was initially hypothesized to have moderately high levels of activity, has shown to have higher normalized mean values than NREM in most, but not all, cases.

A one-way ANOVA test (Matlab 2020b, ‘multcompare’), with TukeyKramer post-hoc comparisons, revealed that there were statistically significant differences between the three states in all the experimental animals (Figure 7 - 13) mostly as well as between individually compared normalized mean values. Each experimental animal has shown that the normalized mean for REM was significantly different from the other two sleep states ($p<0.05$). Comparing wake and NREM, we found that in most cases when wake had a higher normalized mean value, there was a statistical difference between the two groups ($p<0.05$). Furthermore, only one animal was shown to have statistical difference when the NREM mean value was higher than wake. This may be due to an off-target fiber placement that would lead to the recording of a different region, emphasizing the importance of histological analysis.

The next immediate step pertinent to these results is to perform histological processing to correctly identify the region of injection and fiber placement to indicate that these changes in neuronal signal are in the SuM Nos1 population, versus another adjacent Nos1 group. Overall, on target effects are likely given that this Nos1 group is large and has few large groups of Nos1 neurons nearby. In any case, if the anatomical placement was not accurate, this may imply there are Nos1 neuronal populations near the fiber optic that have a function in promoting wakefulness or REM.

Discussion:

We found a highly significant relationship between Nos1 neuronal activity and REM sleep, as hypothesized based on the chemogenetic and lesion studies of our laboratory and the Luppi group, respectively (Pedersen et al., 2017; Renouard et al., 2015). While not analyzed for the thesis project, we also observed that cellular activity in Nos1 neurons began to increase

before the onset of REM sleep, perhaps suggesting a role in state switching, or at least in being driven early in the state switching process, which is thought to involve the sublaterodorsal nucleus and periaqueductal region (Saper et al., 2010; Scammell, Arrigoni and Lipton, 2017).

In all areas of the brain that were recorded, REM sleep was associated with higher levels of activity. However, due to the absence of histological information about the where the injection and fiber were placed, conclusions are hard to reach as the experimental animals that have conflicting results regarding wake versus NREM activity may be due to being off target and recording from a different area.

Future Directions:

There are three major projects related to this work that will continue after my candidature. Firstly, examining the circuits of REM sleep by examining Nos1-specific projections, particularly to the lateral septal area. Based on data shown here, as well as neuroanatomical tracing, we speculate that REM theta activity is controlled by a circuit including the projection of Nos1 SuM neurons to the ventral subnucleus of the lateral septal area.

We will need to confirm that REM-related increases in activity are limited to Nos1 neurons. We will test this by examining known non-Nos1 GABAergic neurons of the SuM (Pedersen et al., 2017), as well as by examining all neurons of the region. Through the use of fiber photometry, the next steps that would be initiated would be to identify the different neuronal activity of the other distinct cell types that exist in the SuM. To target the Vgat neurons in the SuM, Vgat–Cre transgenic mice will be injected with the same vector, AAV9-Syn-Flex- jGCaMP7s-WPRE. On the other hand, to understand the activity the Vglut2 neurons, wild type mice will be injected with AAV9-Syn-jGCaMP7s-WPRE GCaMP7s vector in the medial SuM. This will record the bulk

fluorescence of the SuM and then, we can further compare the activity of Vglut2 neurons by observing the activity of the other two cell types. In addition, the Vgat/vglut2 neurons are known to greatly innervate into the dentate gyrus which has theorized to act as a "gate" to overexcitation of the hippocampus which could ultimately lead to seizures Thus, the Vgat neurons would be recorded through fiber photometry from mice undergoing the intra-amygdala Kainic acid model of seizures to further understand the role of these neurons.

Lastly, given the strong anti-seizure properties of REM sleep, presumably based on the differing phase relationship of other theta firing principal neurons in the hippocampus (Mizuseki and Buzsaki, 2013), we hypothesize that Nos1 neurons may actually suppress seizures arising in the hippocampal network.

Given the projection of Nos1 neurons of the SuM to the lateral septal area, and given that Renouard et al. (2015) showed decreased theta, but not REM sleep duration, we think these neurons are the cellular basis for the long-appreciated role of the SuM in theta generation. Relatedly, we also noted that there are fluctuation of SuM Nos1 activity during wake and we hypothesize that both in wake and REM, fluctuations in activity may correlate to changes in the well-characterized change in peak theta frequency in the hippocampus (e.g. Vanderwolf, 1969) – something that we will examine with the present data.

From what can be concluded, we can to a certain degree agree with our hypothesis that nitric oxide neurons of the SuM are most potently activated during REM and moderately during wake.

Technical Difficulties:

Due to the appearance of COVID-19 and the limited access to the laboratory, there were delays in various aspects in this project. There were limited resources in not only processing the data

but also analyzing the data. Furthermore, due to the social distancing, there was not enough time to process the brains and section them for anatomical validation of the injection and fiber optic. Thus, the results placed in the thesis needs to be further verified so the signals recorded come from accurate targeting of the desired deep brain region (SuM). The animals with off target injections and fiber placements are our control animals as we are able to compare the signals recorded to those found in the anatomically valid animals.

Appendix

Custom MATLAB Script for Raw Signal Processing and Analysis

```
load('NPM 587 - Sleep Score with Demodulated Data.mat')

%CHANGE to relevant channels
Ch13=FP_EEG_EMG_REC_NPM587_200214_154710_000_Ch13; %Sleep scores
Ch21=FP_EEG_EMG_REC_NPM587_200214_154710_000_Ch21; %405 nm
Ch22=FP_EEG_EMG_REC_NPM587_200214_154710_000_Ch22; %465 nm

%save npm587 Ch13 Ch21 Ch22
%load npm587

%%
%CHANGE below to asign channels to control, photometry data, sleep score
%scores
c=Ch21.values; %Control
y=Ch22.values; %Data
t=Ch13.times; %sleep times
codes=Ch13.codes(:,1); %sleep codes
Fs=1/Ch21.interval %~3K sampling rate
%%
x=[1:length(y)]'/Fs;

%design low pass filter
Fc=5; %10 Hz and below

[b a]=butter(6,Fc/(Fs/2),'low'); %butterworth

disp('Smoothing')
ySmooth=filtfilt(b,a,y);
cSmooth=filtfilt(b,a,c);

%%
%Regress control onto experimental and subtract - doesn't work well.
% n=length(x);
% coeff=regress(ySmooth,[zSmooth ones(n,1)]);
% yFit=coeff(1)*z+coeff(2);

%Fitting a polynomial works better
%coeff=polyfit(x,cSmooth,2); %fit to control

coeff=polyfit(x,ySmooth,2); % fit to experimental

yFit=polyval(coeff,x);
```

```
%Convert to z-score
% err=ySmooth-cFit; %error
% stdErr=std(err); %compute standard devation
%
% z=(ySmooth-cFit)/stdErr;

yCorrected=ySmooth-yFit;

%normalize data from 0 to 1
yNormalized=yCorrected-min(yCorrected);
yNormalized=yNormalized/max(yNormalized);


%%
%Change 'ind' to show different data -
%MATLAB struggles to plot all data at
%once
%ind=1:length(x); % All data
ind=find(x<2000); %First 2000 s
%ind=find(x>2000 & x<4000); 2nd 2000 s

disp('Plotting')
num=4;
figure
subplot(num,1,1)
hold on
plot(x(ind),y(ind),'g')
plot(x(ind),ySmooth(ind),'r')
plot(x(ind),yFit(ind),'k')
ylim([-0.01 0.05])
leg=legend('Raw','Smooth','Baseline');
set(leg,'Location','Southeast')
ylabel('Experimental')


subplot(num,1,2)
hold on
plot(x(ind),c(ind),'g')
plot(x(ind),cSmooth(ind),'r')
%plot(x(ind),cFit(ind),'k')
ylim([-0.01 0.05])
ylabel('Control')
leg=legend('Raw','Smooth');
set(leg,'Location','Southeast')
```

```
% subplot(num,1,3)
% hold on
% plot(x(ind),z(ind),'b')
% plot([x(ind(1)) x(ind(end))],[2 2],'k:')
% ylim([-3 5])
% %plot([0 x(end)],[2.5 2.5],'r--')
% ylabel('Z Score')

%plot baseline correct
subplot(num,1,3)
plot(x(ind),yNormalized(ind),'b')
ylabel('Normalized')


%plot sleep
subplot(num,1,4)
plot(t,codes,'k.-')
hold on
xlim([0 x(ind(end))])
ylim([0 4])
ylabel('Sleep Score')
xlabel('Time (s)')
text(1300,3,'1=Awake, 2=Non-REM, 3=REM')


set(gcf,'Color','w')

%%
%Compute mean nomralized data for each sleep score
for i=1:3
    ind=find(codes==i);
    tSmall=t(ind);
    tSmall=tSmall(tSmall<max(x)); %trim off excess
    xInd=round((tSmall+1)*Fs);

    meanY(i)=mean(yNormalized(xInd));
    numCode(i)=length(ind);
    stdErr(i)=std(yNormalized(xInd))/sqrt(length(ind));
end
disp('Mean normalized')
disp(meanY)

disp('Std Err normalized')
disp(stdErr)
```

```
%%
%Match data values to sleep scores
ind=find(t<max(x));
tSmall=t(ind);
codeSmall=codes(ind);
xInd=round((tSmall+1)*Fs);

ySmoothSmall=ySmooth(xInd);
yFitSmall=yFit(xInd);
yNormSmall=yNormalized(xInd);


figure
subplot(311)
plot(tSmall,ySmoothSmall,'r')
hold on
plot(tSmall,yFitSmall,'k')
leg=legend('Smooth','Baseline');
set(leg,'Location','Northeast')
ylabel('Experimental')
title('Entire dataset')


subplot(312)
%plot(tSmall,zSmall)
plot(tSmall,yNormSmall)
ylabel('Normalized')

subplot(313)
plot(tSmall,codeSmall,'k-')
ylim([0 4])
ylabel('Code')
xlabel('Time (s)')

%%


%ANOVA raw data
figure
[p,tbl,stats]=anova1(yNormSmall,codeSmall,'off');
anovaTbl=tbl
cRaw=multcompare(stats);
ylabel('Code')
title('Normalized means')
xlim([0 1])
```

```
disp('Group P-values:')
%cRaw(:,[1:2 6])
p12=cRaw(1,6)
p23=cRaw(2,6)
p13=cRaw(3,6)
```

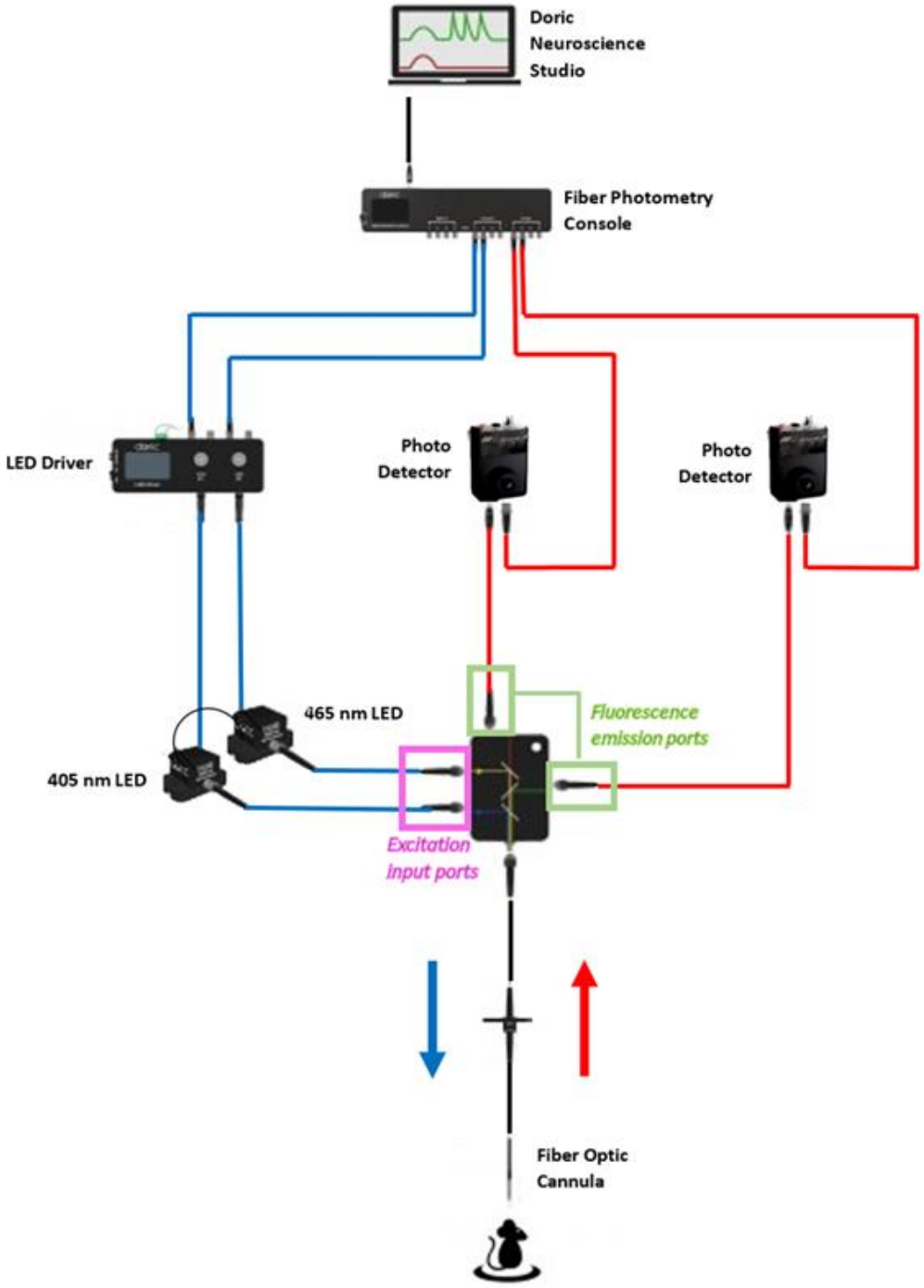

Figure 1: Schematic of the Fiber Photometry Set up.

Modified from Doric Lenses original image of 1 site Fiber photometry

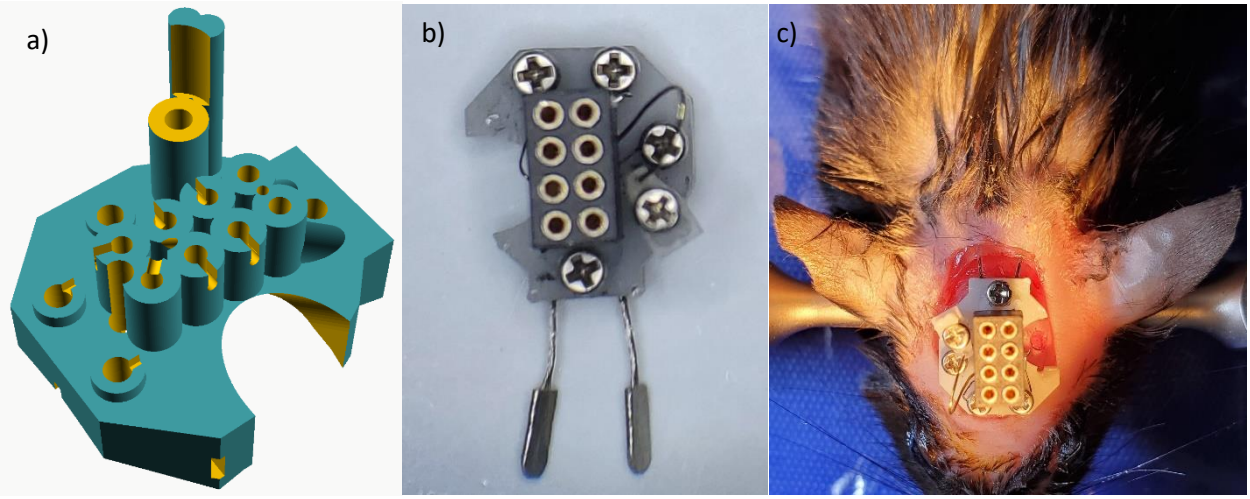

Figure 2: Headplate

a) Above view of the CAD model of the headplate b) Fully assembled headplate ready for placement on mouse c) Placement of headplate onto mouse through stereotaxic surgery

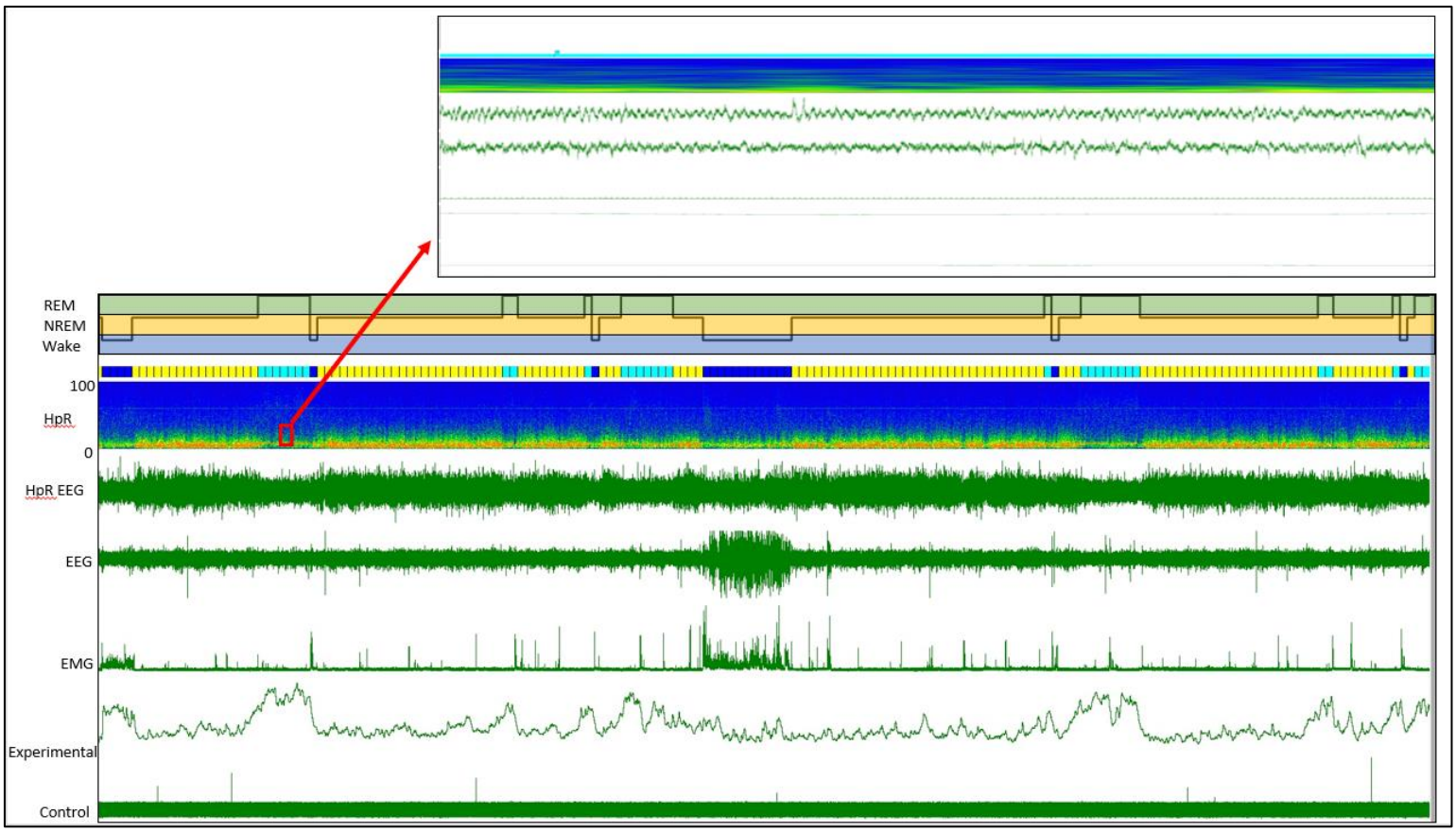

Figure 3: Modified hypnogram and physiological data from 24 hour recording

a) 3600 second trace of Spike2 recording including a Fast Fourier Transform of the HpR (Hippocampus) is shown in color representing power and frequency with a range of 0 to 100 Hz. Correlated EMG signal is shown alongside two smoothed fiber photometry signals. 30 second tracing during REM sleep within the same 3600 second span.

Figure 4: Comparison between processed raw data and demodulated data

Smoothed raw fiber photometry signal observed in ch5 is visibly similar to the demodulated signal in Ch4 obtained through Doric neuroscience studio. The Pearson r value was computed between the two signals (r = 0.99).

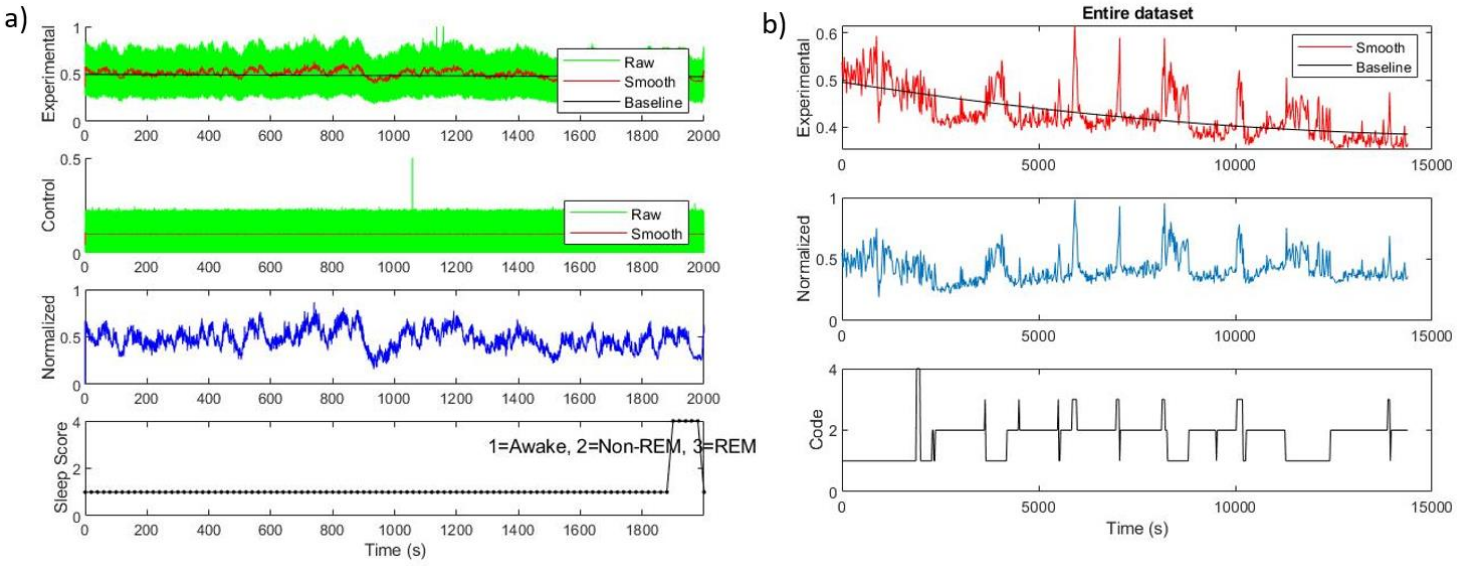

Figure 5: Raw Signal Processing for NPM 603

a) Processing of experimental raw signal through the use of smoothing and baseline correction. Control signal was not baseline corrected due to its stability over time. Experimental signal is normalized. b) 4 hour experimental recording that undergoes smoothing, baseline correction and normalization. (Bottom) Hypnogram that indicates the 3 different states of sleep and wake during the four hour recording. *4 is a doubt channel and is not significant considered in the analysis

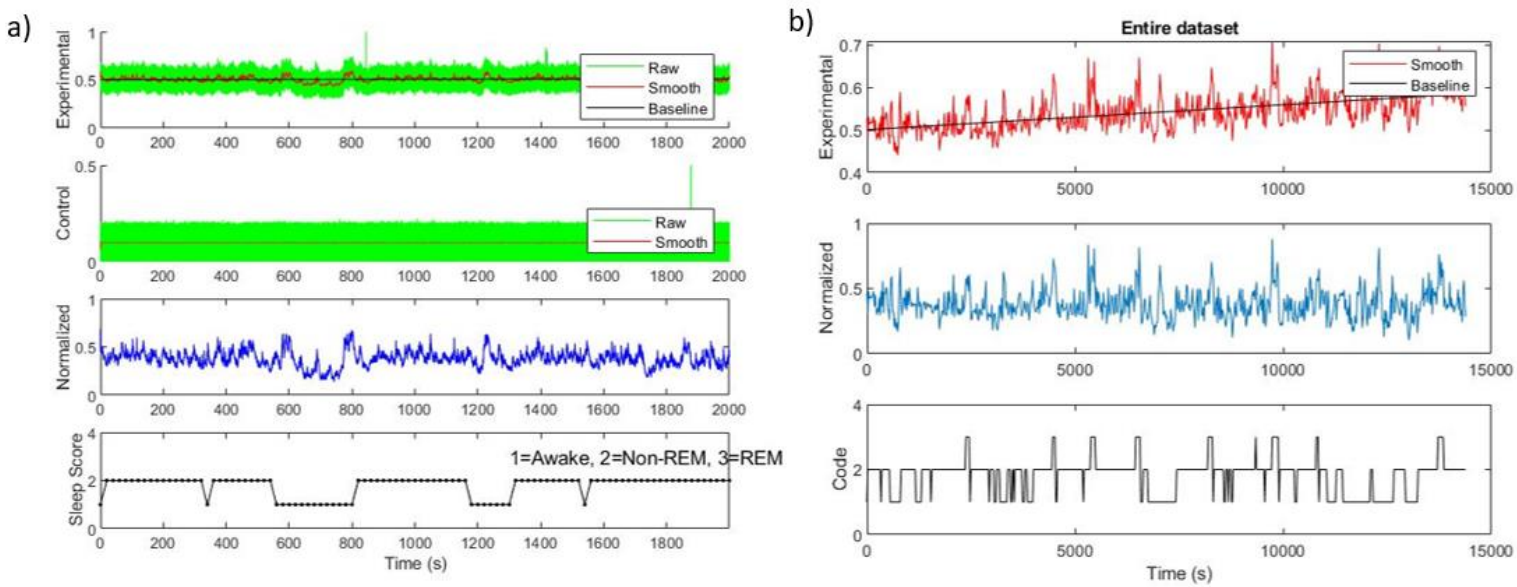

Figure 6: Raw Signal Processing for 598

a) Processing of experimental raw signal through the use of smoothing and baseline correction. Control signal was not baseline corrected due to its stability over time. Experimental signal is normalized. b) 4 hour experimental recording that undergoes smoothing, baseline correction and normalization. (Bottom) Hypnogram that indicates the 3 different states of sleep and wake during the four hour recording.

a)

NPM 603	Normalized Mean	Normalized SEM
1 (Wake)	0.4942	0.0077
2 (NREM)	0.3667	0.0028
3 (REM)	0.6306	0.0311

b)

Source	SS	df	MS	F	Prob>F
Groups	4.02381	3	1.34127	183.84	2.24889e-88
Error	5.22391	716	0.0073		
Total	9.24771	719			

c)

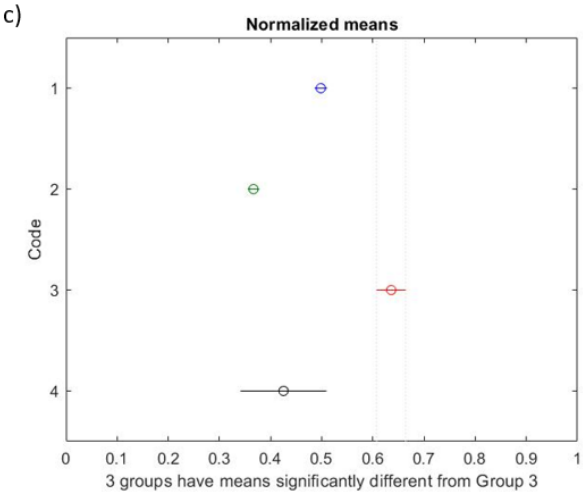

d)

NPM 603	p-value
p12	3.7683E-09
p13	3.7683E-09
p23	3.7683E-09

Figure 7: Data Analysis for NPM 603

a) Table of normalized mean and SEM values for the three different states. Wake mean value is greater than that of NREM b) 1 way ANOVA test results indicated a statistically significant difference among the three groups ($F = 103.84$, $p<0.05$). *4 was a doubt channel and is not significant for the analysis c) Graph of Normalized mean and SEM values for the different states. d) Results from post hoc Tukey-Kramer test and shows that individual sleep states are significantly different from each other ($p<0.05$).

a)

NPM 598	Normalized Mean	Normalized SEM
1 (Wake)	0.3466	0.01
2 (NREM)	0.3704	0.0038
3 (REM)	0.6077	0.0155

b)

Source	SS	df	MS	F	Prob>F
Groups	2.56766	2	1.28383	128.54	1.95595e-48
Error	7.16106	717	0.00999		
Total	9.72872	719			

c)

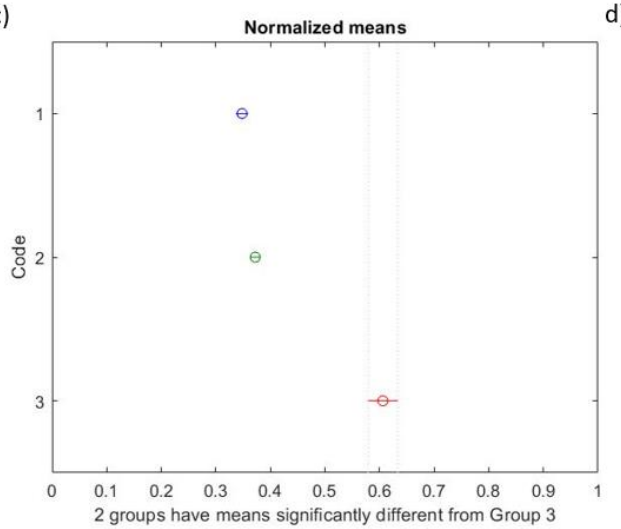

d)

NPM 598	p-value
p12	0.0143
p13	9.5606E-10
p23	9.5606E-10

Figure 8: Data Analysis for NPM 598

a) Table of normalized mean and SEM values for the three different states. In this case, NREM mean value is greater than that of Wake. b) 1 way ANOVA test results indicated a statistically significant difference among the three groups ($F = 120.54$, $p<0.05$). c) Graph of Normalized mean and SEM values for the different states. d) Results from post hoc Tukey-Kramer test and shows that individual sleep states are significantly different from each other ($p<0.05$).

a)

NPM 587	Normalized Mean	Normalized SEM
1 (Wake)	0.3766	0.0097
2 (NREM)	0.3219	0.0073
3 (REM)	0.6411	0.0186

b)

Source	SS	df	MS	F	Prob>F
Groups	6.5753	2	3.28767	235.16	2.96518e-79
Error	10.0242	717	0.01398		
Total	16.5996	719			

c)

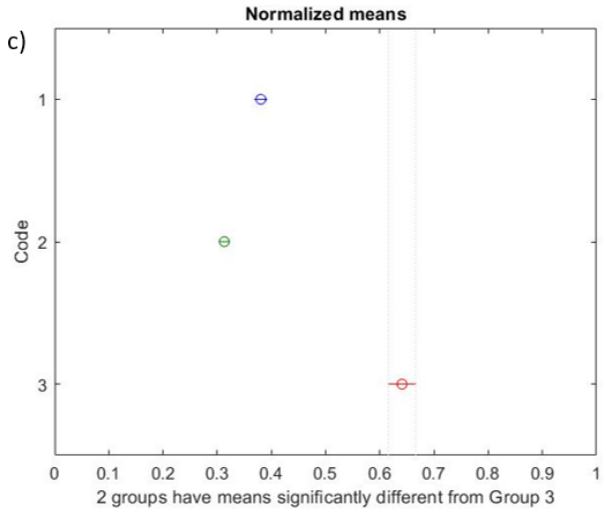

d)

NPM 587	p-value
p_{12}	9.6377E-10
p_{13}	9.5606E-10
p_{23}	9.5606E-10

Figure 9: Data Analysis for NPM 587

a) Table of normalized mean and SEM values for the three different states. In this case, Wake mean value is greater than that of NREM. b) 1 way ANOVA test results indicated a statistically significant difference among the three groups ($F = 235.16$, $p<0.05$). c) Graph of Normalized mean and SEM values for the different states. d) Results from post hoc Tukey-Kramer test and shows that individual sleep states are significantly different from each other ($p<0.05$).

a)

NPM 588	Normalized Mean	Normalized SEM
1 (Wake)	0.2594	0.0069
2 (NREM)	0.2527	0.0065
3 (REM)	0.5586	0.0305

b)

Source	SS	df	MS	F	Prob>F
Groups	2.43418	2	1.21709	120.15	9.98358e-46
Error	7.26329	717	0.01013		
Total	9.69747	719			

c)

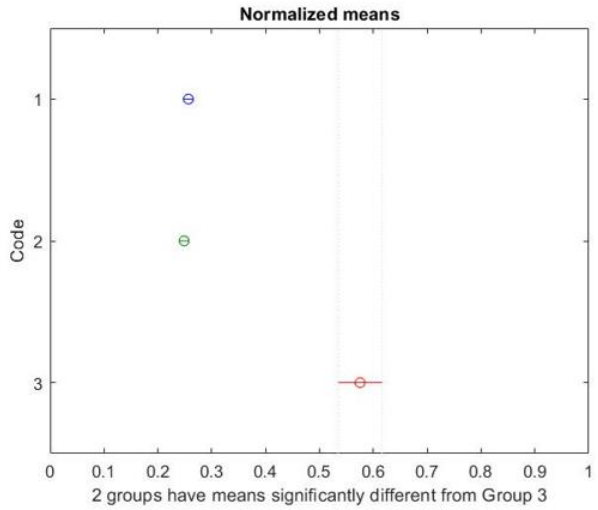

d)

NPM 588	p-value
p_{12}	0.5466
p_{13}	9.5606E-10
p_{23}	9.5606E-10

Figure 10: Data Analysis for NPM 588

a) Table of normalized mean and SEM values for the three different states. In this case, Wake mean value is greater than that of NREM. b) 1 way ANOVA test results indicated a statistically significant difference among the three groups ($F = 120.15$, $p<0.05$). c) Graph of Normalized mean and SEM values for the different states. d) Results from post hoc Tukey-Kramer test and shows while REM significantly differed from the other two states ($p<0.05$), NREM and wake were not significantly different. from each other.

a)

NPM 597	Normalized Mean	Normalized SEM
1 (Wake)	0.4081	0.0092
2 (NREM)	0.3309	0.0056
3 (REM)	0.4655	0.0136

b)

Source	SS	df	MS	F	Prob>F
Groups	1.7051	2	0.85255	96.1	1.06061e-37
Error	6.36112	717	0.00887		
Total	8.06623	719			

c)

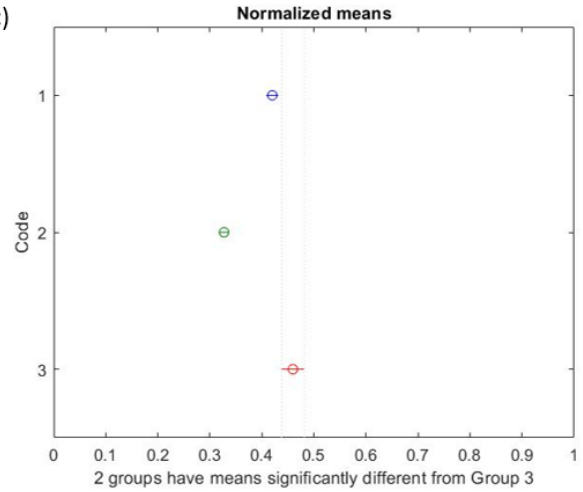

d)

NPM 597	p-value
p_{12}	9.5606E-10
p_{13}	0.0155
p_{23}	9.5606E-10

Figure 11: Data Analysis for NPM 597

a) Table of normalized mean and SEM values for the three different states. In this case, Wake mean value is greater than that of NREM. b) 1 way ANOVA test results indicated a statistically significant difference among the three groups ($F = 96.1$, $p<0.01$). c) Graph of Normalized mean and SEM values for the different states. d) Results from post hoc Tukey-Kramer test that the individual sleep states were significantly different from each other ($p<0.05$).

a)

NPM 600	Normalized Mean	Normalized SEM
1 (Wake)	0.299	0.0096
2 (NREM)	0.3155	0.0047
3 (REM)	0.6215	0.0269

b)

Source	SS	df	MS	F	Prob>F
Groups	6.1302	3	2.04339	28.84	1.30401e-17
Error	50.732	716	0.07085		
Total	56.8621	719			

c)

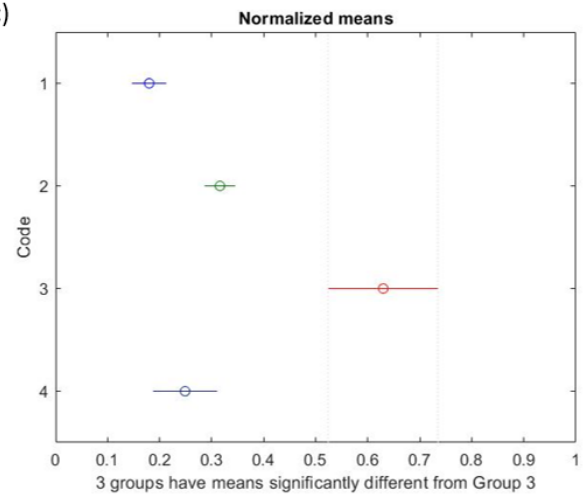

d)

NPM 600	p-value
p12	6.4965E-09
p13	3.7683E-09
p23	3.8576E-08

Figure 12: Data Analysis for NPM 600

a) Table of normalized mean and SEM values for the three different states. In this case, NREM mean value is greater than that of Wake. b) 1 way ANOVA test results indicated a statistically significant difference among the three groups ($F = 26.64$, $p<0.01$). c) Graph of Normalized mean and SEM values for the different states. d) Results from post hoc Tukey-Kramer test that the individual sleep states were significantly different from each other ($p<0.05$).

a)

NPM 602	Normalized Mean	Normalized SEM
1 (Wake)	0.3098	0.0124
2 (NREM)	0.2416	0.0033
3 (REM)	0.5803	0.0293

b)

Source	SS	df	MS	F	Prob>F
Groups	3.79409	2	1.89705	232.69	1.31838e-78
Error	5.84546	717	0.00815		
Total	9.63955	719			

c)

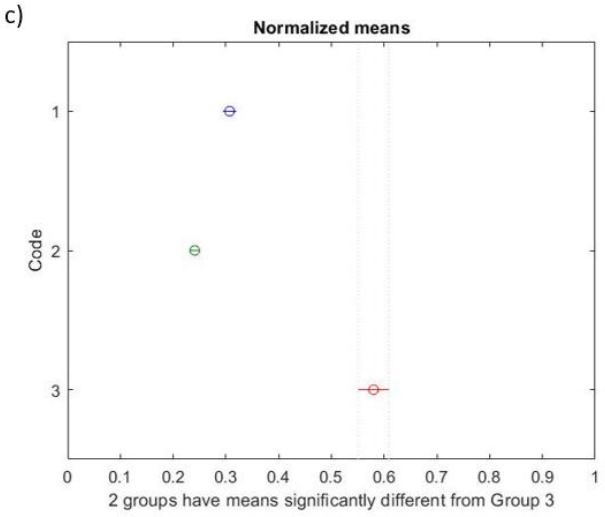

d)

NPM 602	p-value
p12	9.6059E-10
p13	9.5606E-10
p23	9.5606E-10

Figure 13: Data Analysis for NPM 602

a) Table of normalized mean and SEM values for the three different states. In this case, Wake mean value is greater than that of NREM. b) 1 way ANOVA test results indicated a statistically significant difference among the three groups ($F = 232.69$, $p<0.01$). c) Graph of Normalized mean and SEM values for the different states. d) Results from post hoc Tukey-Kramer test that the individual sleep states were significantly different from each other ($p<0.05$).

References:

Akerboom J, Chen TW, Wardill TJ, Tian L, Marvin JS, Mutlu S, Calderón NC, Esposti F, Borghuis BG, Sun XR, Gordus A, Orger MB, Portugues R, Engert F, Macklin JJ, Filosa A, Aggarwal A, Kerr RA, Takagi R, Kracun S, Shigetomi E, Khakh BS, Baier H, Lagnado L, Wang SS, Bargmann CI, Kimmel BE, Jayaraman V, Svoboda K, Kim DS, Schreiter ER, Looger LL. Optimization of a GCaMP calcium indicator for neural activity imaging. J Neurosci. 2012 Oct 3;32(40):13819-40.

Amaral DG, Cowan WM. Subcortical afferents to the hippocampal formation in the monkey. J. Comp Neurol. 1980 Feb 15;189(4):573-91.

Anaclet, C., Pedersen, N. P., Ferrari, L. L., Venner, A., Bass, C. E., Arrigoni, E., & Fuller, P. M. (2015). Basal forebrain control of wakefulness and cortical rhythms. Nature communications, 6, 8744.

Aston-Jones G, Chiang C, Alexinsky T. Discharge of noradrenergic locuscoeruleus neurons in behaving rats and monkeys suggests a role in vigilance. Prog Brain Res. 1991;88:501-20. Review.

Batini C, Moruzzi G, Palestini M, Rossi GF, Zanchetti A. Effects of complete pontine transections on the sleep-wakefulness rhythm: the midpontine pretri-geminal preparation. Arch Ital Biol. 1959;97:1–12.

Billwiller F, Renouard L, Clement O, Fort P, Luppi PH. Differential origin of the activation of dorsal and ventral dentate gyrus granule cells during paradoxical (REM) sleep in the rat. Brain Struct Funct. 2017;222(3):1495-507.

Blumberg MS, Coleman CM, Gerth AI, McMurray B. Spatiotemporal structure of REM sleep twitching reveals developmental origins of motor synergies. Curr Biol. 2013;23:2100–2109.

Blumberg MS, Marques HG, Iida F. Twitching in sensorimotor development from sleeping rats to robots. Curr Biol. 2013;23:R532–R537.

Blumberg MS, Seelke AM. The form and function of infant sleep: from muscle to neocortex. In: Blumberg MS, Freeman JH, Robinson SR, editors. Oxford Handbook of Developmental Behavioral Neuroscience. Oxford University Press; 2010. pp. 391–423

Carskadon MA, Dement WC. Normal human sleep: An overview. Philadelphia: Elsevier Saunders; 2005. pp. 13–23.

Chen TW, Wardill TJ, Sun Y, Pulver SR, Renninger SL, Baohan A, Schreiter ER, Kerr RA, Orger MB, Jayaraman V, Looger LL, Svoboda K, Kim DS. Ultrasensitive fluorescent proteins for imaging neuronal activity. Nature. 2013 Jul 18;499(7458):295-300.

Costa-Miserachs D, Portell-Cortés I, Torras-Garcia M, Morgado-Bernal I. Automated sleep staging in rat with a standard spreadsheet. J Neurosci Methods. 2003 Nov 30;130(1):93-101.

Dana, H., Sun, Y., Mohar, B. et al. High-performance calcium sensors for imaging activity in neuronal populations and microcompartments. Nat Methods 16, 649–657 (2019).

Diekelmann, S., Born, J. The memory function of sleep. Nat Rev Neurosci 11, 114–126 (2010)

Eban-Rothschild A, Rothschild G, Giardino WJ, Jones JR, de Lecea L. VTA dopaminergic neurons regulate ethologically relevant sleep-wake behaviors. Nat Neurosci. 2016;19(10):1356-66.

Edley SM, Graybiel AM. The afferent and efferent connections of the feline nucleus tegmenti pedunculopontinus, pars compacta. J Comp Neurol. 1983 Jun 20;217(2):187-215

El Mansari, M., Sakai, K. & Jouvet, M. Unitary characteristics of presumptive cholinergic tegmental neurons during the sleep-waking cycle in freely moving cats. Exp Brain Res 76, 519–529 (1989).

Fischer DB, Boes AD, Demertzi A, Evrard HC, Laureys S, Edlow BL, Liu H, Saper CB, Pascual-Leone A, Fox MD, Geerling JC. A human brain network derived from coma-causing brainstem lesions. Neurology. 2016 Dec 6;87(23):2427-2434.

French JD, Magoun HW. Effects of chronic lesions in central cephalic brain stem of monkeys. AMA Arch Neurol Psychiatry. 1952 Nov;68(5):591-604.

Fuller, Patrick M et al. “Reassessment of the structural basis of the ascending arousal system.” The Journal of comparative neurology vol. 519,5 (2011): 933-56.

Gao V, Turek F, Vitaterna M. Multiple classifier systems for automatic sleep scoring in mice. J Neurosci Methods. 2016 May 1;264:33-39.

Groenewegen HJ, Berendse HW. The specificity of the 'nonspecific' midline and intralaminar thalamic nuclei. Trends Neurosci. 1994 Feb;17(2):52-7.

Gunaydin LA, Grosenick L, Finkelstein JC, Kauvar IV, Fenno LE, Adhikari A, et al. Natural neural projection dynamics underlying social behavior. Cell. 2014;157(7):1535-51.

Hallanger AE, Wainer BH. Ascending projections from the pedunculopontine tegmental nucleus and the adjacent mesopontine tegmentum in the rat. J Comp Neurol. 1988 Aug 22;274(4):483-515.

Ito HT, Moser EI, Moser MB. Supramammillary Nucleus Modulates Spike-Time Coordination in the Prefrontal-Thalamo-Hippocampal Circuit during Navigation. Neuron. 2018;99(3):576-87 e5.

Kadam SD, D'Ambrosio R, Duveau V, Roucard C, Garcia-Cairasco N, Ikeda A, et al. Methodological standards and interpretation of video-electroencephalography in adult control rodents. A TASK1-WG1 report of the AES/ILAE Translational Task Force of the ILAE. French JA, Galanopoulou AS, O'Brien TJ, Simonato M, editors. Epilepsia. 3rd ed. 2017 Nov 6;58(Suppl. 4):10–27.

Kerr R, Lev-Ram V, Baird G, Vincent P, Tsien RY, Schafer WR. Optical imaging of calcium transients in neurons and pharyngeal muscle of C. elegans. Neuron. 2000 Jun;26(3):583-94.

Klemm WR. Why does REM sleep occur? A wake-up hypothesis. Front Syst Neurosci. 2011;5:73.

Krook-Magnuson E, Armstrong C, Bui A, Lew S, Oijala M, Soltesz I. In vivo evaluation of the dentate gate theory in epilepsy. J Physiol. 2015;593(10):2379-88

Lee MG, Hassani OK, Alonso A, Jones BE. Cholinergic basal forebrain neurons burst with theta during waking and paradoxical sleep. J Neurosci. 2005;25:4365–9

Lee MG, Manns ID, Alonso A, Jones BE. Sleep-wake related discharge properties of basal forebrain neurons recorded with micropipettes in head-fixed rats. J Neurophysiol. 2004;92:1182–9.

Li Y, Bao H, Luo Y, Yoan C, Sullivan HA, Quintanilla L, Wickersham I, Lazarus M, Shin YI, Song J (2020). Supramammillary nucleus synchronizes with dentate gyrus to regulate spatial memory retrieval through glutamate release. eLife, 9, e53129.

Lindsley DB, Bowden JW, Magoun HW. Effect upon the EEG of acute injury to the brain stem activating system. Electroencephalogr Clin Neurophysiol. 1949 Nov;1(4):475-86.

Lindsley DB, Schreiner LH, Knowles WB, Magoun HW. Behavioral and EEG changes following chronic brain stem lesions in the cat. Electroencephalogr Clin Neurophysiol. 1950 Nov;2(4):483-98.

McGinty DJ, Harper RM. Dorsal raphe neurons: depression of firing during sleep in cats. Brain Res. 1976 Jan 23;101(3):569-75.

Mizuseki K, Buzsáki G. Preconfigured, skewed distribution of firing rates in the hippocampus and entorhinal cortex. Cell Rep. 2013 Sep 12;4(5):1010-21.

Morison RS, Dempsey EW.A study of thalamo-cortical relations. Am J Physiol Content. 1941; 135: 281-292

Moruzzi G, Magoun HW. Brain stem reticular formation and activation of the EEG. Electroencephalogr Clin Neurophysiol. 1949 Nov;1(4):455-73.

Nauta WJH. Hypothalamic regulation of sleep in rats. An experimental study. J Neurophysiol. 1946;9:285–314.

Nauta WJH, Kuypers HGJM. Some ascending pathways in the brainstem reticular formation. In: Jasper H, editor. The Reticular Formation of the Brain. Little Brown; Boston: 1958. pp. 3–30.

Olszewski J, Baxter D. Cytoarchitecture of the human brainstem. J Comp Neurol. 1954;101(3):825.

Pan WX, McNaughton N. The supramammillary area: its organization, functions and relationship to the hippocampus. Prog Neurobiol. 2004 Oct;74(3):127-66. Review.

Parvizi J, Damasio A. Consciousness and the brainstem. Cognition. 2001 Apr;79(1-2):135-60

Pedersen, N.P., Ferrari, L., Venner, A. et al. Supramammillary glutamate neurons are a key node of the arousal system. Nat Commun 8, 1405 (2017).

Periasamy S, Hsu DZ, Fu YH, Liu MY. Sleep deprivation-induced multi-organ injury: role of oxidative stress and inflammation. EXCLI Journal. 2015;14:672–683.

Purves D, Augustine GJ, Fitzpatrick D, et al., editors. Neuroscience. 2nd edition. Sunderland (MA): Sinauer Associates; 2001. Stages of Sleep.

Ranson SW, Somnolence caused by hypothalamic lesions in the monkey Arch. Neurol. Psychiatry, 41 (1939), pp. 1-23

Renouard L, Billwiller F, Ogawa K, Clément O, Camargo N, Abdelkarim M, Gay N, Scoté-Blachon C, Touré R, Libourel PA, Ravassard P, Salvert D, Peyron C, Claustrat B, Léger L, Salin P, Malleret G, Fort P, Luppi PH. The supramammillary nucleus and the claustrum activate the cortex during REM sleep. Sci Adv. 2015 Apr3;1(3):e1400177.

Sabatini BL, Oertner TG, Svoboda K. The life cycle of Ca(2+) ions in dendritic spines. Neuron. 2002;33:439–452.

Saper, CB, Chou, TC, Scammell TE. (2001). The sleep switch: Hypothalamic control of sleep and wakefulness. Trends in Neurosciences, 24(12), 726–731.

Saper CB. Organization of cerebral cortical afferent systems in the rat. II. Hypothalamocortical projections. J Comp Neurol. 1985 Jul 1;237(1):21-46.

Saper CB. Diffuse cortical projection systems: anatomical organization and role in cortical function F. Plum (Ed.), Handbook of Physiology. The Nervous System V, American Physiology Society (1987), pp. 169-210

Scammell TE, Arrigoni E, Lipton JO. Neural Circuitry of Wakefulness and Sleep. Neuron. 2017 Feb 22;93(4):747-765.

Schnütgen F, Doerflinger N, Calléja C, Wendling O, Chambon P, Ghyselinck NB. A directional strategy for monitoring Cre-mediated recombination at the cellular level in the mouse. Nat Biotechnol. 2003 May;21(5):562-5.

Shahidi S, Motamedi F, Naghdi N. Effect of reversible inactivation of the supramammillary nucleus on spatial learning and memory in rats. Brain Res. 2004;1026(2):267-74.

Shahidi S, Motamedi F, Bakeshloo SA, Taleghani BK. The effect of reversible inactivation of the supramammillary nucleus on passive avoidance learning in rats. Behav Brain Res. 2004;152(1):81-7.

Sherin JE, Shiromani PJ, McCarley RW, Saper CB. Activation of ventrolateral preoptic neurons during sleep. Science. 1996 Jan 12;271(5246):216-9.

Shouse MN, Farber PR, Staba RJ. Physiological basis: how NREM sleep components can promote and REM sleep components can suppress seizure discharge propagation. Clin Neurophysiol. 2000 Sep;111 Suppl 2:S9-S18.

Siegel JM. Clues to the functions of mammalian sleep. Nature. 2005 Oct 27;437(7063):1264-71.

Steriade M, McCormick DA, Sejnowski TJ. Thalamocortical oscillations in the sleeping and aroused brain. Science. 1993;262:679–85.

Vanderwolf CH. Hippocampal electrical activity and voluntary movement in the rat. Electroencephalogr Clin Neurophysiol. 1969 Apr;26(4):407-18.

Vanni-Mercier G, Sakai K, Jouvet M. Specific neurons for wakefulness in the posterior hypothalamus in the cat Comptes Rendus de L'academie des sciences. Serie III, Sciences de la vie. 1984 ;298(7):195-200.

Vilensky JA, The compendium of anatomical variants: 2011, *Clinical Anatomy*, **24**, 8, (937-937), (2011).

Von Economo, Constantin Freiherr. "Encephalitis lethargica." (1917): 581-583.

Weitzman, E. (1972). “Periodicity in sleep and waking states,” in The Sleeping Brain. Perspectives in the Brain Sciences, Vol. 1, ed. M. H. Chase (Los Angeles: University of California), 193–238.

Zhu KJ, Aiani LM, Pedersen NP. Reconfigurable 3D-Printed headplates for reproducible and rapid implantation of EEG, EMG and depth electrodes in mice. J Neurosci Methods. 2020 Mar 1;333:108566.